Theory of temperature-dependent consumer-resource interactions

Alexis Synodinos, B. Haegeman, Arnaud Sentis, José Montoya

Title: Theory of temperature-dependent consumer-resource interactions

Running head: Temperature-dependence of consumer-resource interactions

Keywords: climate change, consumer-resource dynamics, food webs, community stability, biomass distributions, interaction strength, temperature dependence.

Article Type: Ideas and Perspectives

Authors: Alexis D. Synodinos[1*], Bart Haegeman[1], Arnaud Sentis[2], José M. Montoya[1]

[1]Theoretical and Experimental Ecology Station, CNRS, Moulis, 09200, France

[2]INRAE, Aix Marseille Univ., UMR RECOVER, 3275 route Cézanne, 13182 Aix-en-Provence, France.

* Correspondence to

Alexios Synodinos, Theoretical and Experimental Ecology Station, UMR 5321, 2 Route du CNRS, Moulis, 09200, France, Tel : +33 561 04 05 89, email : alexios.synodinos@sete.cnrs.fr

Author emails:

Bart Haegeman: bart.haegeman@sete.cnrs.fr

Arnaud Sentis: arnaud.sentis@inrae.fr

José M. Montoya: josemaria.montoyateran@sete.cnrs.fr

Author contributions: ADS, BH, AS and JMM conceived the approach. ADS and BH developed the method, AS and JMM guided its application. ADS led the writing of the manuscript; BH, AS and JMM provided crucial input and guidance throughout the writing process. JMM obtained the funding and managed the project. The authors declare no competing interests.

Data accessibility statement: This study produced no new data. Any data used was taken from existing publication and is detailed in the Supplementary Information.

Number of words in Abstract: 191

Number of words in main text (excluding abstract, figure and table legends, acknowledgments and references): 7,441

Number of references: 73

Number of figures: 7

Number of tables: 1

Abstract

Changes in temperature affect consumer-resource interactions, which underpin the functioning of ecosystems. However, existing studies report contrasting predictions regarding the impacts of warming on biological rates and community dynamics. To improve prediction accuracy and comparability, we develop an approach that combines sensitivity analysis and aggregate parameters. The former determines which biological parameters impact the community most strongly at a given temperature. The use of aggregate parameters (i.e., maximal energetic efficiency, ρ, and interaction strength, κ), that combine multiple biological parameters, increases explanatory power and reduces the complexity of theoretical analyses. We illustrate the approach using empirically-derived thermal dependence curves of biological rates and applying it to consumer-resource biomass ratio and community stability. Based on our analyses, we generate four predictions: 1) resource growth rate regulates biomass distributions at mild temperatures, 2) interaction strength alone determines the thermal boundaries of the community, 3) warming destabilises dynamics at low and mild temperatures only, 4) interactions strength must decrease faster than maximal energetic efficiency for warming to stabilise dynamics. We argue for the potential benefits of directly working with the aggregate parameters to increase the accuracy of predictions on warming impacts on food webs and promote cross-system comparisons.

Introduction

Temperature strongly regulates consumer-resource interactions that constitute the fundamental blocks of ecosystems (O'Connor *et al.* 2009; Montoya & Raffaelli 2010; Petchey *et al.* 2010; Rall *et al.* 2012; Amarasekare 2019), and anthropogenic climate change will, in most cases, increase mean temperatures (*IPCC 2013*). Therefore, understanding and predicting the impacts of warming on consumer-resource interactions has attracted much interest (Vasseur & McCann 2005; Binzer *et al.* 2012; Thakur *et al.* 2017). A breakthrough occurred with the postulation that metabolic rate increases exponentially with temperature, with the slope (often referred to as activation energy) conserved across levels of organisation (Gilooly *et al.* 2001; Brown *et al.* 2004). However, activation energies can vary significantly among organisms and biological rates (Dell *et al.* 2011; Réveillon *et al.* 2019). In addition, the thermal response curve of biological rates can decrease at high temperatures, producing a unimodal thermal dependence shape (Deutsch *et al.* 2008; Pörtner & Farrell 2008; Englund *et al.* 2011; Uiterwaal & DeLong 2020). This lack of consensus regarding the exact shape of the temperature-dependence of physiological rates (e.g. ingestion rates), behavioural traits (e.g. consumer search or attack rates) or production (carrying capacity) has contributed to diverging, sometimes contradicting, predictions of how consumer-resource interactions will respond to warming (e.g. Vucic-Pestic *et al.* 2011; Sentis *et al.* 2012).

A dual approach to address the divergence in predictions

Two community properties describing important features of the community are consumer-resource biomass ratio and stability, defined with respect to the occurrence of oscillations. Their importance is reflected in their prevalence in the literature on the effects of warming on

92 consumer-resource communities and food webs (Rall *et al.* 2010, 2012; Uszko *et al.* 2017;
93 Barbier & Loreau 2019; Bideault *et al.* 2020). However, predictions vary about the impacts
94 of warming on both these community properties. Biomass ratios have been theorised to
95 increase (Rip & McCann 2011; Gilbert *et al.* 2014) or decrease (Vasseur & McCann 2005)
96 monotonically with warming, though experimentally-derived data have mainly yield
97 unimodal responses (Fussmann *et al.* 2014; Uszko *et al.* 2017). Likewise, the effects of
98 warming on stability remain unclear. Using data on specific rates (e.g. consumer ingestion
99 and metabolism), studies have inferred that stability either increases monotonically (Rall *et*
100 *al.* 2010, 2012; Vucic-Pestic *et al.* 2011; Fussmann *et al.* 2014) or responds unimodally
101 (Sentis *et al.* 2012; Betini *et al.* 2019) to warming. Theoretical work on stability, in particular
102 on the mechanisms causing the onset of oscillations, expands decades (Rosenzweig &
103 MacArthur 1963; May 1972). Vasseur and McCann (2005) showed that warming will
104 destabilise consumer-resource communities when the consumer metabolic rate increases
105 slower than the ingestion rate. Johnson and Amarasekare (2015) demonstrated the pivotal
106 role of the temperature-dependence of carrying capacity — rather than metabolism and
107 ingestion — in determining warming-stability relationships. All these examples demonstrate
108 that the mixed predictions, whether empirically-derived or theoretical, originate from two
109 distinct sources: the different parameters hypothesised to be driving community responses
110 and the thermal dependence shapes of these parameters. To improve the accuracy of
111 predictions regarding the effects of warming on consumer-resource communities, we need to
112 establish which biological parameters drive community properties (biomass distribution,
113 stability) and to acquire a mechanistic understanding of how their thermal dependence shapes
114 affect community properties.
115

A dual approach utilising sensitivity analysis and the application of aggregate parameters can address both these issues (Fig. 1). On the one hand, sensitivity analysis establishes the parameters that most strongly influence the community property of interest: it quantifies the incremental increase in a response variable with respect to a small incremental increase in a parameter. It has been extensively used in population ecology and demography (Caswell 2019), with important applications in applied ecology (Manlik *et al.* 2018). Since the relative importance of parameters can change along the temperature gradient, a sensitivity analysis allows us to determine the temperatures at which changes in the values of the different parameters have the strongest relative impact (Zhao *et al.* 2020).

On the other hand, we can aggregate groups of the primary parameters into fewer, biologically meaningful and empirically measurable quantities. The use of such aggregate parameters reduces the complexity of theoretical analyses, provides a mechanistic interpretation for the difference in predictions and facilitates the comparison among predictions (Barbier & Loreau 2019; Bideault *et al.* 2020). Experimentally, replacing multiple measurements of individual parameters with measurements of the aggregates could also restrict the room for divergent findings. The seminal work of Yodzis and Innes (1992) reduced the analysis of consumer-resource interactions to two principal aggregate parameters; consumer maximal energetic efficiency and a measure of resource abundance. A variation of maximal energetic efficiency (termed energetic efficiency) has been widely used by empirical studies. However, rather than being measured directly, it has been derived from measurements of its principle components, i.e., feeding and metabolic rates (Rall *et al.* 2010; Vucic-Pestic *et al.* 2011; Sentis *et al.* 2012). Gilbert et al. (2014) posited that a single aggregate parameter — interaction strength defined as the impact of the consumer on the resource population density — could capture the effects of warming on the stability of

consumer-resource interactions. However, their approach was based on a type I (non-saturating) functional response, whereas most consumer-resource species pairs typically produce type II or III (saturating) functional responses (Jeschke *et al.* 2004). Moreover, the thermal dependence of interaction strength did not match the impact of warming on stability for type II or III functional responses (Uszko *et al.* 2017), pointing to a more complex relationship between interaction strength, warming and stability. We use two aggregate parameters: the maximal energetic efficiency of the consumer population, defined as the ratio of energetic gains through ingestion with no resource limitation (i.e., maximal energetic gains) over energetic losses associated to metabolic demand (Yodzis & Innes 1992) and interaction strength, measured as the ratio of resource population density without consumers to resource population density with consumers (Gilbert *et al.* 2014).

Thus, our dual approach identifies the parameters causing the divergence in predictions through the sensitivity analysis and simplifies complex theoretical explorations and empirical measurements through the two aggregate parameters (Fig. 1). By expressing the sensitivities and the community dynamics in terms of the aggregate parameters, analyses collapse into two dimensions. This creates a simple and mechanistic tool to increase the accuracy and improve comparability of theoretical and empirically-driven predictions on the impact of temperature changes on consumer-resource communities. The dual approach of sensitivity analysis and parameter aggregation is not tailored to a specific model of consumer-resource interactions as both are often used independently for different ecological models (e.g. Barbier et al., add a ref for sensitivity). Here, we apply this general approach to the Rosenzweig-MacArthur model (Rosenzweig & MacArthur 1963), a model frequently used to study the effects of temperature on consumer-resource interactions (Fussmann *et al.* 2014; Uszko *et al.* 2017; Daugaard *et al.* 2019; Dee *et al.* 2020). Moreover, our approach can be applied to both static

and dynamic properties of consumer-resource interactions. We illustrate this application using consumer-resource biomass ratio and a stability metric quantifying the proximity to oscillations, respectively; these two variables dominating the literature on the effects of warming on consumer-resource communities (Vasseur & McCann 2005; Rall *et al.* 2008; Uszko *et al.* 2017; Betini *et al.* 2019). We implement different thermal parameterisations from the literature to elucidate how the relative importance of different parameters and their varying thermal dependence shapes impact predicted effects of temperature on consumer-resource interactions. Based on our results, we make four predictions that can be theoretically and empirically tested.

The dual approach

In this study we illustrate the application of the dual approach (i.e. parameter sensitivity and aggregation) using the Rosenzweig-MacArthur model with a type II functional response (Rosenzweig & MacArthur 1963). This model describes the rate of change in resource and consumer biomass densities:

$$\frac{dR}{dt} = r(1 - \frac{R}{K})R - \frac{aR}{1+ahR}C \quad (1)$$

$$\frac{dC}{dt} = (e\frac{aR}{1+ahR} - m)C \quad (2)$$

R and C are the resource and consumer species biomass densities, respectively. Resource growth is logistic, with an intrinsic growth rate, r, and carrying capacity, K. Resource biomass density is limited by the consumer through a saturating Holling type II functional response with attack rate, a, and handling time, h. Consumer growth is proportional to the

191 assimilated consumed biomass, with *e* the dimensionless assimilation efficiency; losses occur
192 due to metabolic costs, *m*. Below we present the formulas most relevant to our study; an
193 extensive analysis of the model is available in the supplementary information (SI 1). We
194 chose a type II response due to its prevalence in many natural consumer-resource interactions
195 (Jeschke *et al.* 2004), though our approach works for the general form of the functional
196 response (SI 2). Additionally, the functional response can be defined with respect to attack
197 rate and handing time, $f(R) = \frac{aR}{1+ahR}$, or maximum consumption rate, *J*, and half-saturation
198 density, R_0, $f(R) = \frac{JR}{R_0+R}$ (SI 3).
199
200 *Stability and aggregate parameters*
201
202 As demonstrated through the 'paradox of enrichment' (Rosenzweig 1971), the Rosenzweig-
203 MacArthur model produces population cycles (oscillations) with increasing energy fluxes
204 (Rip & McCann 2011). Therefore, the coexistence equilibrium can be stable or unstable,
205 where dynamics oscillate around the unstable equilibrium (i.e., a limit cycle). The switch
206 from stable to unstable dynamics occurs at a Hopf bifurcation. Theoretical studies have
207 analysed this qualitative change (Yodzis & Innes 1992; Vasseur & McCann 2005;
208 Amarasekare 2015) because these distinct stability regimes translate to different temporal
209 dynamics, with oscillations leading to greater variability over time. We applied a stability
210 metric that quantifies the tendency of the dynamics to oscillate (Johnson & Amarasekare
211 2015).
212
213 For our analyses we assumed dynamics had converged to the stable equilibrium or the limit
214 cycle and determined the coexistence equilibria and the biomass ratio analytically (SI 1).
215 Equilibrium means zero rate of change for both consumer and resource population biomasses.

For the limit cycle, this yields the unstable equilibrium which is approximately equal to the time-averaged biomass values along the limit cycle. Thus, we set equations (1) and (2) to zero, solved to yield the coexistence equilibrium and retrieved the biomass ratio:

$$\mathcal{B} = \frac{C_S}{R_S} = er\frac{aK(e-mh)-m}{amK(e-mh)} \qquad (3)$$

In the model analysis we observed certain repeated parameter groupings (i.e., aggregate parameters) governed the dynamics (SI 1). Such aggregates have been previously used for the analysis of the Rosenzweig-MacArthur model (Yodzis & Innes 1992; Vasseur & McCann 2005). The aggregates we selected represent ecological mechanisms which can be empirically measured. These are maximal energetic efficiency, $\rho = \frac{e}{mh}$, and interaction strength, $\kappa = ahK\left(\frac{e}{mh} - 1\right)$. A closer look at ρ and κ elucidates their biological meaning. $\frac{1}{h}$ is the saturation value of the functional response and thus represents the maximum consumption rate, J. Hence, ρ can be written as:

$$\rho = \underbrace{e}_{\substack{consumer\\ assimilation\\ efficiecny}} * \underbrace{J}_{\substack{maximum\\ consumption\ rate}} * \underbrace{\frac{1}{m}}_{\substack{consumer\\ metabolic\\ loss}} = \frac{maximal\ energetic\ gain}{energetic\ loss}$$

ρ quantifies the energetic gain-to-loss ratio of the consumer population biomass assuming its maximum feeding rate is realised (i.e. unlimited resources). ρ was introduced by Yodzis and Innes (1992) as a key aggregate parameter to understand food web dynamics. In empirical studies, a variant of ρ termed energetic efficiency, y, has been often applied (Rall *et al.* 2010; Sentis *et al.* 2012, 2017). Unlike ρ, y is a function of the full functional response term and

hence also depends on resource density, $y = \frac{e*f(R)}{m}$, where $f(R) = \frac{aR}{1+ahR}$ at a specified resource density, *R*.

The second aggregate parameter, κ, can be rewritten in terms of the resource population density:

$$\kappa = ahK\left(\frac{e}{mh} - 1\right) = \frac{K}{R_S}$$

κ is the ratio of the resource equilibrium density without consumers (carrying capacity) to the resource equilibrium density with consumers. κ quantifies the effect of the consumer population on the resource population and measures interaction strength (Berlow *et al.* 1999; Gilbert *et al.* 2014).

Using ρ and κ we determine the conditions for positive resource (eq. 4) and consumer (eq. 5) densities, as well as the Hopf bifurcation (eq. 6) (SI 1):

$$\rho > 1 \qquad (4)$$

$$\kappa > 1 \qquad (5)$$

$$\kappa - \rho - 1 = 0 \qquad (6)$$

κ>1 requires that ρ>1 (SI 1). Hence, κ>*1* defines the consumer feasibility boundary. We do not consider stochastic extinctions which may occur due to large-amplitude oscillations when population biomass reaches very low values.

To determine stability, we adjusted the metric of Johnson and Amarasekare (2015) so that it vanished at the Hopf bifurcation (SI 4). This metric, $\mathcal{S}$, defines stability solely in relation to the Hopf bifurcation.

$$\mathcal{S} = -\frac{(\kappa - \rho - 1)}{\rho - 1}$$

$\mathcal{S}>0$ corresponds to a stable equilibrium and $\mathcal{S}<0$ to oscillations.

Sensitivity analysis

We performed a sensitivity analysis of the biomass ratio ($\mathcal{B}$) and the stability metric ($\mathcal{S}$) with respect to the original model parameters (i.e., r, a, h, e and m). A sensitivity analysis quantifies the effect of an infinitesimal change in a parameter on the response variable. Typically, while one parameter is being perturbed, all others are assumed to remain constant and correlations between the parameters are not explicitly considered. However, this approach can be applied in cases of correlated parameter change without a loss of accuracy. As many environmental conditions (e.g. temperature) induce correlated changes in the parameters , then the sensitivity of the response variable (e.g. $\mathcal{B}$ or $\mathcal{S}$) with respect to the environmental conditions can be reconstructed by combining the sensitivities of the individual parameters (SI 5.1). Different types of sensitivity indices exist such as simple sensitivity and elasticity (Manlik *et al.* 2018; Caswell 2019). Here we used elasticity for

biomass ratio ($\mathcal{B}$) and an adjusted elasticity for stability ($\mathcal{S}$) (SI 5.1), both dimensionless to facilitate direct comparisons between parameter sensitivities.

Elasticity is a proportional sensitivity, quantifying how a relative change in a parameter translates into a relative change in the variable; otherwise known as the log-scaled sensitivity (Manlik *et al.* 2018). Thus, the elasticity of $\mathcal{B}$ with respect to parameter x is given by:

$$\partial_x \mathcal{B} = \frac{\frac{\partial \mathcal{B}}{\mathcal{B}}}{\frac{\partial x}{x}} = \frac{\partial \ln(\mathcal{B})}{\partial \ln(x)}$$

If $\partial_x \mathcal{B}=1$, a relative increase of 10% in parameter x causes a relative increase of 10% in variable $\mathcal{B}$. Conversely, $\partial_x \mathcal{B}=-1$ implies that a relative increase of 10% in parameter x results in relative decrease of 10% in $\mathcal{B}$.

For the sensitivity of the stability metric, $\mathcal{S}$, we used a variation of the elasticity. We defined the sensitivity of $\mathcal{S}$ as the incremental change in $\mathcal{S}$ induced by a relative change in parameter x. Our adjustment was possible due to $\mathcal{S}$ being dimensionless and it prevents sensitivities from diverging to infinity close to the Hopf bifurcation without altering the outcome of our analysis (SI 5.1).

$$\partial_x \mathcal{S} = \frac{\frac{\partial \mathcal{S}}{\partial x}}{\frac{}{x}} = \frac{\partial \mathcal{S}}{\partial \ln(x)}$$

$\partial_x \mathcal{S}=1$ implies that a relative increase in parameter x of 10% translates into an absolute increase of 0.1 in $\mathcal{S}$ and has a stabilising effect. If, conversely, $\partial_x \mathcal{S}=-1$, the same relative increase in x would lead to decrease of 0.1 in $\mathcal{S}$ with a destabilising effect.

The magnitude and sign of each sensitivity determine how strongly and in what direction the parameter perturbation impacts the variable, respectively. We used the magnitudes to rank the relative importance of all parameters. The sign provided qualitative information regarding the direction of change (increasing or decreasing the response variable).

All sensitivities could be expressed in terms of ρ and κ. Hence, sensitivities are fully determined in a plane with of ρ and κ as axes (Fig. SI 5.1, 5.2). In this ρ-κ plane the sensitivities of all parameters can be ranked by magnitude, splitting the parameter space into regions where different parameters have the highest, second highest, etc. sensitivity magnitude. Here, we present figures where the regions are determined by the top-two ranked sensitivities; we do not portray changes in the rankings of the lowest sensitivities (see Fig. SI 5.4 and SI 5.5 for the complete biomass ratio and stability metric regions, respectively). The biomass ratio and stability metric have different sensitivity expressions and, therefore, produced different regions. For each variable, the regions remain fixed irrespective of the parameterisation used, because the sensitivity expressions stem from the model equations. The ρ-κ plane provides additional information, such as the feasibility boundary (eq. 5) and the position of the Hopf bifurcation (eq. 6).

Temperature parameterisations

To demonstrate the impacts of different parameter thermal dependencies, we implemented temperature parameterisations from the literature. Maintenance respiration rates, m, have been shown to increase exponentially with temperature (Brown *et al.* 2004). The Arrhenius equation is most often used to describe this thermal dependence (Vasseur & McCann 2005; Sentis *et al.* 2017; Uszko *et al.* 2017). However, the thermal response curves of resource growth rate, *r*, attack rate, *a* , and handling time, *h*, have been represented either through the Arrhenius equation (Vasseur & McCann 2005; Binzer *et al.* 2016) or as unimodal functions (Amarasekare 2015; Uszko *et al.* 2017; Zhang *et al.* 2017; Uiterwaal & DeLong 2020; Zhao *et al.* 2020). Carrying capacity, *K* , and consumer assimilation efficiency, *e*, have a less clear connection to temperature (Uszko *et al.* 2017; Dee *et al.* 2020). We selected two parametrisations related to the ongoing debate surrounding the importance of including the decreasing part of the biological rates beyond the optimal temperature (Pawar *et al.* 2016) and used these as an illustrative comparison. The 'unimodal' model had a unimodal parameterisation for *r*, *a* (both hump-shaped) and *h* (U-shaped), the Arrhenius equation for *m* (increasing), and constant *K* and *e* (Uszko *et al.* 2017). We compared this to a 'monotonic' parameterisation where all thermal dependencies (*r, a, m* increasing; *h, K* decreasing) follow the Arrhenius equation and *e* is constant (Fussmann *et al.* 2014). Following this comparison, we plotted four additional parameterisations from the literature onto the ρ-κ plane to broaden the comparison and demonstrate the simplicity of applying the approach to empirically-derived measurements. These consisted of two similar monotonic parameterisations (Vucic-Pestic *et al.* 2011; Binzer *et al.* 2016), one where only *a* was hump-shaped (Sentis *et al.* 2012) and one which though monotonic, included some distinctive thermal dependencies – exponentially increasing *K(T)* and *e(T)* and constant *h* (Archer *et al.* 2019). We provide a description of the studies and details of their parameterisations in the supplementary material (SI 6).

We should note that not all parameterisations included the resource growth rate, r, so the biomass ratio could not be calculated in these cases. However, we could calculate ρ and κ and, hence, the biomass ratio elasticities for all parameterisations. Thus, we could determine how biomass ratio sensitivities to individual parameters changed with warming regardless of the actual biomass ratio values. By including studies which had not measured resource growth or estimated the biomass ratio we broadened the scope of the comparison of the biomass ratio sensitivities. Though this does not represent an exhaustive list of parameterisations, we were restricted to parameterisations which could be used to parametrise the Rosenzweig-MacArthur model with a type II response and whose available parameters could yield ρ and κ. 'Mild' and 'extreme' temperatures, as well as 'close' or 'far' from consumer extinction, are defined relative to each parameterisation's temperature range and feasibility boundaries, respectively. The feasible temperature range was determined by interaction strength ($\kappa>1$) with the temperature extremes corresponding to the point of consumer extinction. This condition assumes that resources have a broader thermal range than consumers (e.g., Rose & Caron 2007; West & Post 2016). If resources go extinct at temperatures consumers could withstand, then the feasibility boundary becomes dependent on resource growth rate, r (Amarasekare 2015). The parameterisations we present come from ectotherms, where environmental temperatures correspond to the organisms' temperatures. However, our approach can be transferred to endotherms as it does not depend on a specific thermal parametrisation.

Sensitivities depend on proximity to thermal boundaries

Biomass ratio: always most sensitive to e and m

We analytically obtained four groups of biomass ratio elasticity magnitudes, $\partial_e \mathcal{B}=|\partial_m \mathcal{B}|$, $\partial_K \mathcal{B}=\partial_a \mathcal{B}$, $\partial_r \mathcal{B}$ and $\partial_h \mathcal{B}$. *e* and *m* always have the largest elasticity and hence the strongest relative impact on the biomass ratio ($\partial_e \mathcal{B}=|\partial_m \mathcal{B}| > \partial_K \mathcal{B}, \partial_a \mathcal{B}, \partial_r \mathcal{B}, |\partial_h \mathcal{B}|$, Table 1). Increasing *e* increases the biomass ratio ($\partial_e \mathcal{B} > 0$), increasing *m* reduces it ($\partial_m \mathcal{B} < 0$). *K* and *a* have equal and positive elasticities ($\partial_K \mathcal{B}=\partial_a \mathcal{B} > 0$), both increasing the biomass ratio. The elasticity of *r* is constant, $\partial_r \mathcal{B}=1$; a directly proportional positive effect on $\mathcal{B}$. Increasing *h* reduces the biomass ratio, $\partial_h \mathcal{B} < 0$. These are general results, independent of any model parameterisation (with temperature or otherwise) following directly from the Rosenzweig-MacArthur model's equations.

Biomass ratio: high r elasticity far from thermal boundaries

Both the 'unimodal' and 'monotonic' temperature parameterisations produced a unimodal biomass ratio thermal dependence (Fig. 2). The unimodal parameterisation induced thermal boundaries to the community at both low (1℃) and high (33℃) temperatures (Fig. 2a). The biomass ratio exceeded 1 for most temperatures (higher consumer than resource biomass), peaked at 14℃ around $\mathcal{B} \approx 5.5$ and decreased rapidly to 0 as it approached both thermal boundaries (low and high temperature extremes). The biomass ratio of the monotonic parameterisation (Fig. 2b) increased with warming from low temperatures, peaked at $\mathcal{B} \approx 0.19$, before decreasing to 0 at high temperatures (27.5℃). The two parameterisations are derived from different systems, hence the different temperature ranges.

In both parameterisations, sensitivity to *e* and *m* was highest throughout (Fig. 2c, d) - as expected from the analytical findings. Elasticities were split into two groups at mild

temperatures: e, m and r had the highest elasticity with $\partial_e \mathcal{B} = |\partial_m \mathcal{B}| \approx \partial_r \mathcal{B} = 1$, while a, h and K elasticities were very low. Approaching the temperature extremes all elasticities besides $\partial_r \mathcal{B}$ diverged; $\partial_h \mathcal{B}$ diverged faster than $\partial_K \mathcal{B} = \partial_a \mathcal{B}$ in the unimodal parameterisation (Fig. 2c), while the opposite occurred in the monotonic one (Fig. 2d).

Expressing the elasticities in terms of ρ and κ (Table 1) reduces the sensitivity analysis to two dimensions. Ranking the elasticity magnitudes creates distinct regions in the ρ-κ plane which correspond to different elasticity ranking orderings and provide a mechanistic overview of which elasticities dominate where (Fig. 3a). e and m always have the highest elasticity, so the three regions reflect changes in the second highest-ranked elasticity. Regions adjacent to consumer extinction ($\kappa = 1$) have high sensitivity to either h (red region) or to a and K (yellow region). r elasticity is highest in the region farthest from consumer extinction (orange region). The two temperature parameterisations were mapped onto this plane by calculating their ρ and κ values (Fig 3b and c). Despite the two trajectories being markedly different, both occupied the region where r ranked second highest for most temperatures. The unimodal parameterisation produced a unimodal trajectory, crossing the consumer extinction threshold at low and high temperatures (Fig. 3b). The monotonic parameterisation's trajectory converged monotonically towards consumer extinction with increasing temperature (Fig. 3c).

All other parameterisations from the literature also occupied the region of high r elasticity for most temperatures, far from their thermal boundaries (Fig. 4). Three monotonic parameterisations produced monotonic trajectories (Fig. 4a, b, c) which started in the region of high r elasticity and converged monotonically towards consumer extinction ($\kappa = 1$). With a hump-shaped thermal dependence of attack rate, a unimodal trajectory emerged (Fig. 4d). At low temperatures it occupied the region of high r elasticity but moved away from consumer

425 extinction. With further warming, the trajectory switched direction and followed the same
426 path as the monotonic parameterisations, crossing the consumer extinction boundary. A
427 unimodal thermal dependence for attack rate (hump-shaped) and handling time (U-shaped)
428 (Fig. 4e), induced extinctions at low and high temperatures imposing a unimodal trajectory.
429 Unlike all previous parameterisations, the trajectory crossed the extinction threshold in the
430 region of high *h* elasticity. The final parameterisation, though monotonic, yielded unimodal
431 trajectories (Fig. 4f). A monotonically increasing *K(T)* (as opposed to decreasing in the other
432 monotonic parameterisations and constant in the unimodal ones) initially forced the trajectory
433 away from consumer extinction, albeit within the region of high *r* elasticity. Consumer
434 energetic efficiency ρ decreased, pushing consumers towards extinction, thus forcing an
435 abrupt decline towards the consumer boundary.
436
437 *Stability most sensitive either to e and m or to a and K*
438
439 Similarly to the biomass ratio, the analytical approach for the stability sensitivities yielded
440 results conserved independently of the temperature parameterisations (Table 1): equal
441 sensitivity magnitudes pairwise for *e* and *m* and for *a* and *K* (i.e., $|\partial_e \mathcal{S}| = \partial_m \mathcal{S}$ and $|\partial_K \mathcal{S}| = |\partial_a \mathcal{S}|$),
442 negative stability sensitivities of *e*, *a* and *K* ($\partial_e \mathcal{S}$, $\partial_a \mathcal{S}$, $\partial_K \mathcal{S} < 0$) implying they destabilise
443 dynamics, a positive sensitivity of *m* ($\partial_m \mathcal{S} > 0$) indicating a stabilising effect. *h* can be either
444 stabilising or destabilising and *r* does not affect the stability regime ($\partial_r \mathcal{S} = 0$).
445
446 The unimodal temperature parameterisation exhibited oscillations ($\mathcal{S} < 0$) over most
447 temperatures (Fig. 5a). Only at low and high thermal extremes did dynamics briefly stabilise
448 prior to consumer extinction. The monotonic temperature parametrisation produced
449 oscillations at low temperatures ($\mathcal{S} < 0$), crossed a Hopf bifurcation at 17℃ and dynamics

were stable ($\mathcal{S}>0$) thereafter (Fig. 5b). In both cases, stability close to consumer extinction was most sensitive to consumer assimilation efficiency, e, and metabolism, m, ($|\partial_e \mathcal{S}|=\partial_m \mathcal{S}$) followed by handling time, h (Fig. 5c, d). Moving away from the thermal boundaries, attack rate, a, and carrying capacity, K, increased in relative importance. Furthest away from the thermal boundaries, stability was most sensitive to changes a and K, followed by h. Even though $\partial_h \mathcal{S}$ did not rank highest in any temperature range, it was a close second both at the temperature extremes (second to $|\partial_e \mathcal{S}|=\partial_m \mathcal{S}$) or furthest away from them (second to $|\partial_K \mathcal{S}|=|\partial_a \mathcal{S}|$). Additionally, h switched from destabilising at mild temperatures ($\partial_h \mathcal{S}<0$) to stabilising ($\partial_h \mathcal{S}>0$) close to the temperature extremes (Fig. 5c, d, Fig. S5.2).

The ρ-κ plane for the stability metric was split into four regions; in two regions closest to consumer extinction, $|\partial_e \mathcal{S}|=\partial_m \mathcal{S}$ were the largest sensitivities (Fig. 6a, red and yellow regions) and in the two regions furthest from consumer extinction, $|\partial_K \mathcal{S}|=|\partial_a \mathcal{S}|$ranked highest (Fig. 6a, green and blue regions). Additionally, the Hopf bifurcation (Fig. 6a, dashed curve) split the plane into stable equilibrium and oscillation regions. Corresponding to the general findings, stability in the two reference ('unimodal' and 'monotonic') parameterisations was most sensitive to changes in e and m at the thermal extremes - close to consumer extinction - and to a and K at milder temperatures – far from consumer extinction (Fig. 6b, c). The unimodal trajectory occupied the region of oscillations for most temperatures, crossing the Hopf bifurcation twice close to consumer extinction, once at low and once at high temperatures (Fig. 6b, blue region). The monotonic trajectory started in the region of oscillations and moved into the stable region with warming, crossing the Hopf bifurcation far from the thermal extreme (Fig. 6c, yellow region).

Parameter thermal dependencies impact warming-stability relationships

Plotting the other temperature parameterisations' trajectories onto the ρ-κ plane reproduced the same patterns with respect to the stability metric's sensitivity (Fig. 7): stability was most sensitive to e and m at the thermal extremes and to a and K far from the extremes. Significantly, the trajectories revealed the impact of the thermal dependence shape of individual parameters on the warming-stability relationship. In three monotonic parameterisations, warming stabilised the dynamics (Fig. 7 a, b, c). In the cases, when oscillations did take place, these occurred at low temperatures (Fig 7a resident prey, b, c) and dynamics crossed the Hopf bifurcation far from the thermal boundary. In the case with two enrichment levels (Fig. 7c), the high enrichment scenario required higher temperatures to stabilise the dynamics. For the unimodal trajectory with hump-shaped attack rate (Fig. 7d), warming at low temperatures pushed the dynamics towards (low enrichment) or deeper into (high enrichment) the region with oscillations (i.e., destabilised dynamics). Here too, the destabilising impact of enrichment was evident. However, further warming switched the direction of the trajectory. Subsequently, both ρ and κ decreased. κ declined much faster, forcing the dynamics towards the stable region and eventually consumer extinction. Both the switch in the trajectory direction and the Hopf bifurcation (high enrichment scenario) occurred at mild temperatures, in the region of high a and K sensitivity. In the parameterisation with both a (hump-shaped) and h (U-shaped) unimodal (Fig. 7e), the Hopf bifurcation occurred close to the thermal boundaries, where κ increased (low temperatures) or decreased (high temperatures) much faster than ρ. The dynamics were oscillatory for most temperatures, with the switch in the trajectory's direction occurring in the region of highest sensitivity to a and K. The final parameterisation's trajectories were characterised by a negative relationship between ρ and κ (Fig. 7f). Driven by the positive thermal dependence of

carrying capacity, warming increased κ and destabilised dynamics which oscillated for most temperatures.

Discussion

Research on the impacts of warming on consumer-resource interactions has yielded mixed results (Vasseur & McCann 2005; Englund *et al.* 2011; Rall *et al.* 2012; Gilbert *et al.* 2014; Uszko *et al.* 2017). Resolving this debate and improving predictions has become even more pressing as most ecosystems face increased temperatures (Easterling *et al.* 2000; Walther *et al.* 2002; Root *et al.* 2003; Parmesan 2006). Here, we developed an approach to improve and simplify predictions on the impacts of warming on consumer-resource interactions. This approach integrates two pathways: (1) a sensitivity analysis to identify the key biological parameters whose variations have the largest relative impact on community properties at a given temperature, and (2) aggregate parameters (maximal energetic efficiency, ρ, and interaction strength, κ) to increase explanatory power. We used the Rosenzweig-MacArthur model with a type II functional response, and applied the approach to consumer-resource biomass ratio and a stability metric quantifying the propensity for oscillations (Johnson & Amarasekare 2015). Therefore, our insights apply to study systems well-described by the Rosenzweig-MacArthur model. Our analyses revealed that the relative significance of different parameter groupings is determined by the proximity of the consumer to its thermal boundaries. We, further, elucidated how differences in the shape of the thermal dependence curves of individual parameters qualitatively impact predictions. We used empirically-derived thermal dependence curves of biological parameters from the literature to illustrate this.

524 We focus our discussion on the formulation of four testable predictions arising from our
525 results. For each prediction, we present its implications and rationale. Then, we discuss the
526 empirical measurement of the aggregate parameters and present important subtleties and
527 potential extensions of our approach.
528
529 *Prediction 1: Resource growth rate regulates biomass distribution at mild temperatures*
530
531 *Implications*: We showed that the relative dominance of consumer assimilation efficiency,
532 metabolism and resource growth rate in driving changes in biomass distributions should
533 manifest itself in any consumer-resource community far from its feasibility boundaries,
534 assuming these communities are well-described by the Rosenzweig-MacArthur model (Fig.
535 3a). Due to the agreement about the thermal dependence of metabolism (Rall *et al.* 2010;
536 Fussmann *et al.* 2014; Uszko *et al.* 2017) and the negligible -if any- change of assimilation
537 efficiency with warming (Dell *et al.* 2011), differences in the thermal performance curve of
538 resource growth rate will strongly impact biomass ratio predictions. Therefore, improved
539 predictions about the impacts of warming on biomass distributions at mild temperatures
540 necessitate the accurate description of the thermal dependence of resource growth rate.
541
542 *Reasoning*: Far from the community thermal boundaries, consumer assimilation efficiency,
543 metabolism and resource growth rate always had the greatest elasticity with an almost equal
544 relative impact on biomass ratio ($\partial_e \mathcal{B} = |\partial_m \mathcal{B}| \approx \partial_r \mathcal{B} = 1$, Fig. 2c, d and Fig. S5.1). Increasing
545 metabolism reduced biomass ratios (Table 1), which is likely to be a universal response
546 across ecosystems, given the positive exponential dependence of metabolism on temperature
547 across organisms (Gilooly *et al.* 2001; Brown *et al.* 2004; Rall *et al.* 2012 but see Ehnes *et al.*
548 2011). Conversely, assimilation efficiency increased biomass ratios but has either been

549 assumed to be unaffected by temperature changes (Vasseur & McCann 2005; Sentis *et al.*
550 2017; Uszko *et al.* 2017) or has yielded a weak temperature-dependence (Wurtsbaugh &
551 Davis 1977; Handeland *et al.* 2008; Lang *et al.* 2017; Daugaard *et al.* 2019) with negligible
552 change compared to other parameters. Increasing resource growth rate also increased the
553 biomass ratio. However, evidence on the shape of resource growth's thermal response
554 remains inconclusive: it can either increase exponentially with temperature (Savage *et al.*
555 2004) or decrease abruptly beyond the thermal optimum (Dannon *et al.* 2010; Thomas *et al.*
556 2012). Since the biomass ratio is directly proportional to the resource growth rate ($\partial_r \mathcal{B}=1$,
557 Table 1), it will be strongly affected by the values and shape of the resource growth rate
558 thermal performance curve. Given the consensus surrounding the temperature-dependence of
559 metabolism and the minor scale of potential change in assimilation efficiency with
560 temperature, our findings emphasise the significance of correctly parameterising the resource
561 growth rate when aiming to predict biomass distribution changes due to warming at mild
562 temperatures.
563
564 *Prediction 2: Interaction strength determines consumer survival with increasing*
565 *temperatures.*
566
567 *Implications*: If resources have a broader thermal range compared to consumers (Rose &
568 Caron 2007; West & Post 2016), the thermal boundaries of the community can be determined
569 by measuring solely the thermal dependence of interaction strength, κ. This quantity — the
570 ratio of the resource equilibrium density without consumers (carrying capacity) to the
571 resource equilibrium density with consumers — can be determined experimentally (Berlow *et*
572 *al.* 2004) or through observations, facilitating predictions and cross-system comparisons
573 thereof.

574

575 *Reasoning*: Close to the consumer extinction boundary, consumer survival becomes
576 extremely sensitive to all parameters apart from resource growth (Fig. 2, S5.1), making
577 accurate predictions challenging. Currently, consumer survival has been inferred through
578 energetic efficiency — the effective energetic gain of consumers at a certain resource density
579 — which requires determining the thermal dependence of the functional response (Vucic-
580 Pestic *et al.* 2011; Archer *et al.* 2019). Not only is the functional response's thermal
581 dependence hotly contested (Uszko *et al.* 2017; Uiterwaal & DeLong 2020), but this
582 uncertainty will be exacerbated by its extremely high sensitivity at the community's thermal
583 boundaries. We showed there exists an alternative, empirically more direct and theoretically
584 more robust metric to determine consumer survival, and hence community feasibility.
585 Interaction strength — the relative values of resource equilibrium without and with
586 consumers (Berlow *et al.* 1999, 2004; Gilbert *et al.* 2014) — provides the necessary condition
587 for consumer survival ($\kappa>1$), when resources are thermal generalists compared to consumers.
588 This provides an accurate threshold and represents a measurable quantity that can be
589 standardised across experimental designs and study systems (Berlow *et al.* 2004).

590

591 *Prediction 3: Warming reduces community stability at low and mild temperatures*

592

593 *Implications*: This prediction rests on important assumptions: that resources have a broader
594 thermal range, that organisms currently experience temperatures below their optima (Pawar
595 *et al.* 2016) and that the functional response is of type II with a unimodal thermal dependence
596 (Rall *et al.* 2012; Sentis *et al.* 2012; Kuiters 2013; West & Post 2016; Uszko *et al.* 2017;
597 Uiterwaal & DeLong 2020). We deem these assumptions realistic based on the literature;

598 therefore, we argue that consumer-resource interactions at low and mild temperatures will be
599 destabilised by warming. At higher temperatures, warming should always enhance stability.
600
601 *Reasoning*: Stability in the context of consumer-resource interactions has predominantly
602 referred to a qualitative distinction between stable and oscillating dynamics (Rosenzweig &
603 MacArthur 1963; Yodzis & Innes 1992; Vasseur & McCann 2005). We based our analysis on
604 an adjusted stability metric which quantifies the tendency of dynamics to oscillate (Johnson
605 & Amarasekare 2015, SI 4). When comparing existing temperature parameterisations, we
606 found that in most monotonic parameterisations (increasing metabolism and attack rate,
607 decreasing handling time and carrying capacity, assimilation efficiency constant), warming
608 always (i.e., monotonically) stabilised dynamics (Fig. 7a, b, c). The single exception arose
609 when warming and carrying capacity increased simultaneously, which destabilised dynamics
610 (Fig. 7f). Carrying capacity has been described as a proxy for enrichment and its destabilising
611 effect has been established whether independently of temperature (Rosenzweig 1971) or as
612 antagonistic to warming (Binzer *et al.* 2016). When at least one parameter in the functional
613 response had a unimodal thermal dependence (i.e., hump-shaped attack rate or U-shaped
614 handling time), this yielded a unimodal warming-stability relationship (Fig. 7d, e).
615 Significantly, the divergence between the unimodal and (most) monotonic parameterisations
616 in the predicted effect of warming on stability manifested itself at low or mild, rather than
617 high temperatures (Fig. 6, 7). This pattern originates in the impact of the parameters with
618 unimodal thermal dependencies on stability. Attack rate is destabilising (Table 1, McCann
619 2011). Thus, a hump-shaped thermal dependence of attack rate destabilises dynamics with
620 warming below the thermal optimum and stabilises dynamics beyond it. Handling time is
621 stabilising close to the thermal extremes (Fig. 6c, S5.2). A U-shaped handling time will
622 rapidly decrease with warming from low temperatures, which is strongly destabilising; a

623 corresponding steep increase at high temperatures produces a strong stabilising effect. Thus,
624 warming at high temperatures will always be stabilising. However, at lower temperatures,
625 unimodal and monotonic thermal dependencies produce contrasting warming-stability
626 relationships. Therefore, the thermal dependence shape of the functional response combined
627 with the temperatures currently experienced by communities relative to their optimal
628 temperature will determine the impact of warming on stability (Betini *et al.* 2019).
629
630 *Prediction 4: Warming stabilises dynamics only when interaction strength decreases faster*
631 *than maximal energetic efficiency*
632
633 *Implications*: The combination of ρ — the energetic gain-to-loss ratio of consumers given
634 unlimited resources — and κ — interaction strength — accurately describes the warming-
635 stability relationship with no recourse to the thermal dependence shapes of individual
636 parameters, the current temperatures relative to the thermal optima, or the proximity to the
637 thermal boundaries of the community. Therefore, differential responses of resources and
638 consumers to warming (Dell *et al.* 2014) will be encompassed by the thermal dependence of
639 the aggregates – assuming the consumer-resource system is well-described by the
640 Rosenzweig-MacArthur model. The Hopf bifurcation condition (eq. 6) dictates that κ should
641 decrease faster than ρ for warming to stabilise consumer-resource interactions. Thus,
642 measuring ρ and κ directly can increase the accuracy of warming-stability predictions and
643 simplify cross-system comparisons.
644
645 *Reasoning*: Decreasing energetic efficiency or interaction strength have been considered
646 equivalent to increasing stability (Rall *et al.* 2008, 2010; Sentis *et al.* 2012). Thus, estimates
647 of consumer energetic efficiency or interaction strength based on empirically-derived thermal

dependence curves of individual rates (e.g. ingestion rate, attack rate, metabolic rate) have been used to infer the impacts of warming on stability (Rall *et al.* 2010, 2012; Vucic-Pestic *et al.* 2011; Fussmann *et al.* 2014). However, this raises two significant issues. On the one hand, even subtle changes in the thermal dependence shapes of individual parameters can yield all possible outcomes (Amarasekare 2015). On the other hand, reducing the analysis of stability to a single aggregate parameter has limitations. Gilbert *et al.* (2014) described the warming-stability relationship with a single aggregate, interaction strength, but their approach was based on a type I functional response and its predictions do not work well in type II or III scenarios (Uszko *et al.* 2017). Johnson and Amarasekare (2015) and Amarasekare (2015) attained a single aggregate parameter to reduce the complexity of their explorations; however, this lacks descriptive power of the dynamics close to the community's thermal boundaries (SI 4). Our analysis in the ρ-κ plane suggests that stability cannot be reduced to a single aggregate parameter nor does a decrease in either one or both of ρ and κ suffice to stabilise dynamics. In fact, both ρ and κ can decrease with warming while dynamics become destabilised. A stabilising effect of warming requires not only a concurrent reduction in ρ and κ, but also the latter to decrease faster. Critically, both ρ and κ represent biological quantities which can be consistently measured across study systems.

Working with the aggregate parameters

Working directly with the two aggregate parameters, maximal consumer energetic efficiency, ρ, and interaction strength, κ, can simplify empirical measurements and improve the accuracy of theoretical predictions, particularly for field data and experiments, as we argue below. To determine the thermal dependence of maximal consumer energetic efficiency and interaction strength, one can measure consumer population growth given unlimited resources and

673 resource population density in presence and absence of consumers at different temperatures,
674 respectively. These measurements can be performed in the lab and the field. Interaction
675 strength is commonly determined in field experiments where consumers are excluded
676 (Berlow *et al.* 2004; Wootton & Emmerson 2005; Novak 2010; Estes *et al.* 2011). Consumer
677 energetic gain-to-loss ratio under effectively unlimited resources is more rarely estimated.
678 However, it can be derived from consumer population net growth and metabolism and
679 mortality, quantities measured commonly in the field and in the lab (Hanson & Peters 1984;
680 Stemberger & Gilbert 1985; Lampert *et al.* 1986). Moreover, confounding factors in field
681 measurements of the population-level aggregates should generate less uncertainty compared
682 to that of measuring multiple individual parameters, where uncertainty propagates and often
683 generates large uncertainty in model predictions (e.g. Sentis *et al.* 2015). Therefore, working
684 directly with the aggregate parameters can be both simpler and lead to more accurate
685 predictions in the field. On the other hand, measuring the individual parameters in the lab has
686 well-established protocols and a history of reliable outputs, with measurements requiring only
687 short-term experiments as opposed to the aggregates.

688

689 The choice between measuring the aggregate or the individual parameters will be informed
690 by the questions and objectives of each study. The aggregates describe population-level
691 mechanisms of consumer-resource interactions, while the individual parameters correspond
692 to physiological or behavioural processes of individual organisms scaled up to the population
693 level. As we argued, the aggregates can provide more accurate predictions for field
694 measurements whereas individual parameters can be accurately measured in the lab. This
695 does raise the question whether measurements in a controlled laboratory environment can
696 represent noisier conditions in the field. It would be useful to compare directly measured

aggregate parameters to aggregate parameter values derived from the individual parameters to determine how well predictions based on individual rates capture the dynamics of the system. Regardless of the choice, our approach provides the tools for both pathways: studies working with individual parameters will benefit from identifying the most important parameters to measure, while aggregate parameter datapoints can be directly mapped onto the ρ-κ landscape.

Subtleties and extensions

The sensitivity analysis quantified the sensitivity of the model variables to infinitesimal parameter changes. Therefore, applying its insights to data should take into consideration the scales of parameters in the temperature range of interest and potential uncertainties in the parameter estimates (Manlik *et al.* 2018, Fig. Sx). Hence, our argument for the reduced significance of the thermal dependence of assimilation efficiency in driving changes in biomass distributions, despite its high sensitivity.

Regarding the stability of consumer-resource interactions, the ρ-κ plane helped visualise the stabilising effect of a type III functional response (Fig. S2.1), which has both theoretical and empirical support (Sarnelle & Wilson 2008; Kalinkat *et al.* 2013; Uszko *et al.* 2017; Daugaard *et al.* 2019). For the type II response, the defining role of the functional response (attack rate) and the carrying capacity has been widely documented (Rosenzweig 1971; Amarasekare 2015; Johnson & Amarasekare 2015; Binzer *et al.* 2016); we add the important caveat that this is the case only far from consumer extinction (Fig. 6a).

721 Finally, relaxing certain assumptions can extend our approach. Considering the scenario
722 where the consumer has a broader thermal niche relative to that of the resource will make the
723 thermal limits of coexistence dependent on resource growth (Amarasekare 2015).
724 Considering the extinction of populations with very low abundances to account for stochastic
725 extinctions can define a realisable coexistence range within the feasible parameter space.
726 Breaking down the original model parameters (e.g. handling time includes the handling and
727 ingestion of prey) could facilitate our understanding of the role of more fundamental
728 physiological processes in the dynamics. Finally, climate change will lead to stronger
729 fluctuations in temperatures (*IPCC 2013*), which have been shown to alter predictions in
730 consumer-resource dynamics (Vasseur *et al.* 2014; Dee *et al.* 2020). This makes the inclusion
731 of temperature variability an important next step.
732
733 **Conclusions**
734
735 Warming will have significant, but as yet uncertain impacts on consumer-resource
736 interactions which underpin the structure and functioning of ecosystems. We presented an
737 approach that will help to improve the accuracy of predictions and reconcile divergent results
738 by facilitating cross-system comparisons. This approach first determines the parameters
739 whose variations have the largest effect on community properties. Second, it simplifies
740 analyses to a two-dimensional plane of mechanistically tractable aggregate parameters;
741 maximal consumer energetic efficiency and interaction strength. Applying it to consumer-
742 resource biomass ratio and stability, we showed that close to the consumer extinction
743 boundary (i.e., at temperature extremes) both variables are most sensitive to changes in
744 consumer assimilation efficiency and metabolism. Far from the boundary (i.e., mild
745 temperatures), biomass ratio is most sensitive to resource growth rate, consumer assimilation

efficiency and metabolism. This yielded our first prediction, that resource growth rate regulates biomass distributions at mild temperatures. The consensus around the thermal dependence of metabolism and the limited potential impact of warming on assimilation efficiency, underscore the importance of correctly measuring the thermal dependence of resource growth rate. Using the two aggregate parameters also simplified the study of important properties of consumer-resource interactions. From this followed our second prediction, that the thermal boundaries of the community are defined by interaction strength alone. In terms of stability, we demonstrated that a unimodal thermal dependence of attack rate or handling time alters predictions of warming-stability relationships below the thermal optimum, where many organisms may be currently living. Hence our third prediction, that initial increases in mean temperatures will destabilise consumer-resource interactions. Significantly, our approach elucidates how the thermal dependence of stability can be comprehensively characterised by maximal energetic efficiency and interaction strength values. This produced our fourth prediction; a faster reduction of interaction strength than of maximal energetic efficiency with warming is necessary for dynamics to stabilise. Finally, we demonstrated the potential for targeted experiments to measure the thermal dependencies of maximal energetic efficiency and interaction strength to improve predictions. Ultimately, we show that any temperature parameterisation fitted to the Rosenzweig-MacArthur model can be mapped onto the aggregate parameter plane, revealing its stability landscape, providing a mechanistic interpretation for its predictions and allowing for the cross-system comparison of these predictions.

Acknowledgments

We thank three anonymous reviewers and the editor for their constructive feedback. This research is supported by the FRAGCLIM Consolidator Grant, funded by the European Research Council under the European Union's Horizon 2020 research and innovation programme (Grant Agreement Number 726176), and by the "Laboratoires d'Excellences (LABEX)" TULIP (ANR-10-LABX-41).

References

Amarasekare, P. (2015). Effects of temperature on consumer-resource interactions. *J. Anim. Ecol.*, 84, 665–679.

Amarasekare, P. (2019). Effects of Climate Warming on Consumer-Resource Interactions: A Latitudinal Perspective. *Front. Ecol. Evol.*, 7.

Archer, L.C., Sohlström, E.H., Gallo, B., Jochum, M., Woodward, G., Kordas, R.L., *et al.* (2019). Consistent temperature dependence of functional response parameters and their use in predicting population abundance. *J. Anim. Ecol.*, 88, 1670–1683.

Barbier, M. & Loreau, M. (2019). Pyramids and cascades: a synthesis of food chain functioning and stability. *Ecol. Lett.*, 22, 405–419.

Berlow, E.L., Navarrete, S.A., Briggs, C.J., Power, M.E. & Menge, B.A. (1999). Quantifying Variation in the Strengths of Species Interactions. *Ecology*, 80, 2206.

Berlow, E.L., Neutel, A.M., Cohen, J.E., De Ruiter, P.C., Ebenman, B., Emmerson, M., *et al.* (2004). Interaction strengths in food webs: Issues and opportunities. *J. Anim. Ecol.*

Betini, G.S., Avgar, T., McCann, K.S. & Fryxell, J.M. (2019). Temperature triggers a non□ linear response in resource–consumer interaction strength. *Ecosphere*, 10.

Bideault, A., Galiana, N., Zelnik, Y.R., Gravel, D., Loreau, M., Barbier, M., *et al.* (2020). Thermal mismatches in biological rates determine trophic control and biomass

795 distribution under warming. *Glob. Chang. Biol.*, gcb.15395.
796 Binzer, A., Guill, C., Brose, U. & Rall, B.C. (2012). The dynamics of food chains under
797 climate change and nutrient enrichment. *Philos. Trans. R. Soc. B Biol. Sci.*, 367, 2935–
798 2944.
799 Binzer, A., Guill, C., Rall, B.C. & Brose, U. (2016). Interactive effects of warming,
800 eutrophication and size structure: impacts on biodiversity and food-web structure. *Glob.*
801 *Chang. Biol.*, 22, 220–227.
802 Brown, J.H., Gillooly, J.F., Allen, A.P., Savage, V.M. & West, G.B. (2004). TOWARD A
803 METABOLIC THEORY OF ECOLOGY. *Ecology*, 85, 1771–1789.
804 Caswell, H. (2019). *Sensitivity Analysis: Matrix Methods in Demography and Ecology*.
805 Demographic Research Monographs. Springer International Publishing, Cham.
806 Dannon, E.A., Tamò, M., van Huis, A. & Dicke, M. (2010). Functional response and life
807 history parameters of Apanteles taragamae, a larval parasitoid of Maruca vitrata.
808 *BioControl*, 55, 363–378.
809 Daugaard, U., Petchey, O.L. & Pennekamp, F. (2019). Warming can destabilize predator–
810 prey interactions by shifting the functional response from Type III to Type II. *J. Anim.*
811 *Ecol.*, 88, 1575–1586.
812 Dee, L.E., Okamtoto, D., Gårdmark, A., Montoya, J.M. & Miller, S.J. (2020). Temperature
813 variability alters the stability and thresholds for collapse of interacting species. *Philos.*
814 *Trans. R. Soc. B Biol. Sci.*, 375, 20190457.
815 Dell, A.I., Pawar, S. & Savage, V.M. (2011). Systematic variation in the temperature
816 dependence of physiological and ecological traits. *Proc. Natl. Acad. Sci. U. S. A.*, 108,
817 10591–10596.
818 Dell, A.I., Pawar, S. & Savage, V.M. (2014). Temperature dependence of trophic interactions
819 are driven by asymmetry of species responses and foraging strategy. *J. Anim. Ecol.*, 83,

820 70–84.

821 Deutsch, C.A., Tewksbury, J.J., Huey, R.B., Sheldon, K.S., Ghalambor, C.K., Haak, D.C., *et*
822 *al.* (2008). Impacts of climate warming on terrestrial ectotherms across latitude. *Proc.*
823 *Natl. Acad. Sci.*, 105, 6668–6672.

824 Easterling, D.R., Meehl, G.A., Parmesan, C., Changnon, S.A., Karl, T.R. & Mearns, L.O.
825 (2000). Climate extremes: observations, modeling, and impacts. *Science*, 289, 2068–
826 2074.

827 Ehnes, R.B., Rall, B.C. & Brose, U. (2011). Phylogenetic grouping, curvature and metabolic
828 scaling in terrestrial invertebrates. *Ecol. Lett.*, 14, 993–1000.

829 Englund, G., Öhlund, G., Hein, C.L. & Diehl, S. (2011). Temperature dependence of the
830 functional response. *Ecol. Lett.*, 14, 914–921.

831 Estes, J.A., Terborgh, J., Brashares, J.S., Power, M.E., Berger, J., Bond, W.J., *et al.* (2011).
832 Trophic downgrading of planet earth. *Science (80-.).*

833 Fussmann, K.E., Schwarzmüller, F., Brose, U., Jousset, A. & Rall, B.C. (2014). Ecological
834 stability in response to warming. *Nat. Clim. Chang.*, 4, 206–210.

835 Gilbert, B., Tunney, T.D., McCann, K.S., DeLong, J.P., Vasseur, D.A., Savage, V., *et al.*
836 (2014). A bioenergetic framework for the temperature dependence of trophic
837 interactions. *Ecol. Lett.*, 17, 902–914.

838 Gilooly, J.F., Brown, J.H., Geoffrey, B.W., Savage, V.M. & Charnov, E.L. (2001). Effects of
839 Size and Temperature on Metabolic Rate. *Science (80-.).*, 293, 2248–2251.

840 Handeland, S.O., Imsland, A.K. & Stefansson, S.O. (2008). The effect of temperature and
841 fish size on growth, feed intake, food conversion efficiency and stomach evacuation rate
842 of Atlantic salmon post-smolts. *Aquaculture*, 283, 36–42.

843 Hanson, J.M. & Peters, R.H. (1984). Empirical prediction of crustacean zooplankton biomass
844 and profundal macrobenthos biomass in lakes. *Can. J. Fish. Aquat. Sci.*, 41, 439–445.

IPCC, 2013: *Climate Change 2013: The Physical Science Basis. Contribution of Working Group I to the Fifth Assessment Report of the Intergovernmental Panel on Climate Change* [Stocker, T.F., D. Qin, G.-K. Plattner, M. Tignor, S.K. Allen, J. Boschung, A. Nauels, Y. Xia, V. Bex and P.M. Midgley (eds.)]. Cambridge University Press, Cambridge, United Kingdom and New York, NY, USA, 1535 pp.Jeschke, J.M., Kopp, M. & Tollrian, R. (2004). Consumer-food systems: Why type I functional responses are exclusive to filter feeders. *Biol. Rev. Camb. Philos. Soc.*

Jeschke, J.M., Kopp, M. & Tollrian, R. (2004). Consumer-food systems: Why type I functional responses are exclusive to filter feeders. *Biol. Rev. Camb. Philos. Soc.*

Johnson, C.A. & Amarasekare, P. (2015). A metric for quantifying the oscillatory tendency of consumer-resource interactions. *Am. Nat.*, 185, 87–99.

Kalinkat, G., Schneider, F.D., Digel, C., Guill, C., Rall, B.C. & Brose, U. (2013). Body masses, functional responses and predator-prey stability. *Ecol. Lett.*, 16, 1126–1134.

Kuiters, A. t. (2013). Diversity–stability relationships in plant communities of contrasting habitats. *J. Veg. Sci.*, 24, 453–462.

Lampert, W., Fleckner, W., Rai, H. & Taylor, B.E. (1986). Phytoplankton control by grazing zooplankton: A study on the spring clear□water phase. *Limnol. Oceanogr.*, 31, 478–490.

Lang, B., Ehnes, R.B., Brose, U. & Rall, B.C. (2017). Temperature and consumer type dependencies of energy flows in natural communities. *Oikos*, 126, 1717–1725.

Manlik, O., Lacy, R.C. & Sherwin, W.B. (2018). Applicability and limitations of sensitivity analyses for wildlife management. *J. Appl. Ecol.*, 55, 1430–1440.

May, R.M. (1972). Limit cycles in predator-prey communities. *Science (80-.).*, 177, 900–902.

McCann, K.S. (2011). *Food Webs (MPB-50) | Princeton University Press*. *Monograpsh Pop*

870 *Bio*. Available at: https://press.princeton.edu/books/paperback/9780691134185/food-
871 webs-mpb-50. Last accessed 10 September 2020.
872 Montoya, J.M. & Raffaelli, D. (2010). Climate change, biotic interactions and ecosystem
873 services. *Philos. Trans. R. Soc. B Biol. Sci.*, 365, 2013–2018.
874 Novak, M. (2010). Estimating interaction strengths in nature: experimental support for an
875 observational approach. *Ecology*, 91, 2394–2405.
876 O'Connor, M.I., Piehler, M.F., Leech, D.M., Anton, A. & Bruno, J.F. (2009). Warming and
877 Resource Availability Shift Food Web Structure and Metabolism. *PLoS Biol.*, 7,
878 e1000178.
879 Parmesan, C. (2006). Ecological and Evolutionary Responses to Recent Climate Change.
880 *Annu. Rev. Ecol. Evol. Syst.*, 37, 637–669.
881 Pawar, S., Dell, A.I., Savage, V.M. & Knies, J.L. (2016). Real versus artificial variation in
882 the thermal sensitivity of biological traits. *Am. Nat.*, 187, E41–E52.
883 Petchey, O.L., Brose, U. & Rall, B.C. (2010). Predicting the effects of temperature on food
884 web connectance. *Philos. Trans. R. Soc. B Biol. Sci.*, 365, 2081–2091.
885 Pörtner, H.O. & Farrell, A.P. (2008). Ecology: Physiology and climate change. *Science (80-.
886).*
887 Rall, B., Guill, C. & Brose, U. (2008). Food-web connectance and predator interference
888 dampen the paradox of enrichment. *Oikos*, 117, 202–213.
889 Rall, B.C., Brose, U., Hartvig, M., Kalinkat, G., Schwarzmüller, F., Vucic-Pestic, O., *et al.*
890 (2012). Universal temperature and body-mass scaling of feeding rates. *Philos. Trans. R.
891 Soc. B Biol. Sci.*, 367, 2923–2934.
892 Rall, B.Ö.C., Vucic-Pestic, O., Ehnes, R.B., EmmersoN, M. & Brose, U. (2010).
893 Temperature, predator-prey interaction strength and population stability. *Glob. Chang.
894 Biol.*, 16, 2145–2157.

Réveillon, T., Rota, T., Chauvet, É., Lecerf, A. & Sentis, A. (2019). Repeatable inter□ individual variation in the thermal sensitivity of metabolic rate. *Oikos*, 128, 1633–1640.

Rip, J.M.K. & McCann, K.S. (2011). Cross-ecosystem differences in stability and the principle of energy flux. *Ecol. Lett.*, 14, 733–740.

Root, T.L., Price, J.T., Hall, K.R., Schneider, S.H., Rosenzweig, C. & Pounds, J.A. (2003). Fingerprints of global warming on wild animals and plants. *Nature*, 421, 57–60.

Rose, J.M. & Caron, D.A. (2007). Does low temperature constrain the growth rates of heterotrophic protists? Evidence and implications for algal blooms in cold waters. *Limnol. Oceanogr.*, 52, 886–895.

Rosenzweig, M.L. (1971). Paradox of Enrichment: Destabilization of Exploitation Ecosystems in Ecological Time. *Science (80-.).*, 171, 385–387.

Rosenzweig, M.L. & MacArthur, R.H. (1963). Graphical Representation and Stability Conditions of Predator-Prey Interactions. *Am. Nat.*, 97, 209–223.

Sarnelle, O. & Wilson, A.E. (2008). Type III Functional Response in Daphnia. *Ecology*, 89, 1723–1732.

Savage, V.M., Gilloly, J.F., Brown, J.H., Charnov, E.L. & Charnov, E.L. (2004). Effects of body size and temperature on population growth. *Am. Nat.*, 163, 429–41.

Sentis, A., Binzer, A. & Boukal, D.S. (2017). Temperature-size responses alter food chain persistence across environmental gradients. *Ecol. Lett.*, 20, 852–862.

Sentis, A., Hemptinne, J.L. & Brodeur, J. (2012). Using functional response modeling to investigate the effect of temperature on predator feeding rate and energetic efficiency. *Oecologia*, 169, 1117–1125.

Sentis, A., Morisson, J. & Boukal, D.S. (2015). Thermal acclimation modulates the impacts of temperature and enrichment on trophic interaction strengths and population dynamics. *Glob. Chang. Biol.*, 21, 3290–3298.

920 Stemberger, R.S. & Gilbert, J.J. (1985). Body Size, Food Concentration, and Population
921 Growth in Planktonic Rotifers. *Ecology*, 66, 1151–1159.
922 Thakur, M.P., Künne, T., Griffin, J.N. & Eisenhauer, N. (2017). Warming magnifies
923 predation and reduces prey coexistence in a model litter arthropod system. *Proc. R. Soc.*
924 *B Biol. Sci.*, 284, 20162570.
925 Thomas, M.K., Kremer, C.T., Klausmeier, C.A. & Litchman, E. (2012). A global pattern of
926 thermal adaptation in marine phytoplankton. *Science (80-.).*, 338, 1085–1088.
927 Uiterwaal, S.F. & DeLong, J.P. (2020). Functional responses are maximized at intermediate
928 temperatures. *Ecology*.
929 Uszko, W., Diehl, S., Englund, G. & Amarasekare, P. (2017). Effects of warming on
930 predator-prey interactions - a resource-based approach and a theoretical synthesis. *Ecol.*
931 *Lett.*, 20, 513–523.
932 Vasseur, D.A., DeLong, J.P., Gilbert, B., Greig, H.S., Harley, C.D.G., McCann, K.S., *et al.*
933 (2014). Increased temperature variation poses a greater risk to species than climate
934 warming. *Proc. R. Soc. B Biol. Sci.*, 281.
935 Vasseur, D.A. & McCann, K.S. (2005). A mechanistic approach for modeling temperature-
936 dependent consumer-resource dynamics. *Am. Nat.*, 166, 184–98.
937 Vucic-Pestic, O., Ehnes, R.B., Rall, B.C. & Brose, U. (2011). Warming up the system: higher
938 predator feeding rates but lower energetic efficiencies. *Glob. Chang. Biol.*, 17, 1301–
939 1310.
940 Walther, G.-R., Post, E., Convey, P., Menzel, A., Parmesan, C., Beebee, T.J.C., *et al.* (2002).
941 Ecological responses to recent climate change. *Nature*, 416, 389–395.
942 West, D.C. & Post, D.M. (2016). Impacts of warming revealed by linking resource growth
943 rates with consumer functional responses. *J. Anim. Ecol.*, 85, 671–680.
944 Wootton, J.T. & Emmerson, M. (2005). Measurement of Interaction Strength in Nature.

945 *Annu. Rev. Ecol. Evol. Syst.*, 36, 419–444.

946 Wurtsbaugh, W.A. & Davis, G.E. (1977). Effects of temperature and ration level on the
947 growth and food conversion efficiency of Salmo gairdneri, Richardson. *J. Fish Biol.*, 11,
948 87–98.

949 Yodzis, P. & Innes, S. (1992). Body size and consumer-resource dynamics. *Am. Nat.*, 139,
950 1151–1175.

951 Zhang, L., Takahashi, D., Hartvig, M. & Andersen, K.H. (2017). Food-web dynamics under
952 climate change. *Proc. R. Soc. B Biol. Sci.*, 284, 20171772.

953 Zhao, Q., Liu, S. & Niu, X. (2020). Effect of water temperature on the dynamic behavior of
954 phytoplankton–zooplankton model. *Appl. Math. Comput.*, 378, 125211.

955 **Tables and Figures**

956

957 Table 1. Sensitivities of the biomass ratio ($\partial_x \mathcal{B}$) and of the stability metric ($\partial_x \mathcal{S}$) with respect
958 to the six original model parameters. All sensitivities are expressed in terms of ρ and κ.

959

Parameter	Consumer-resource biomass ratio, $\mathcal{B}$	Stability metric, $\mathcal{S}$
x	$\partial_x \mathcal{B} = \frac{\partial \ln(\mathcal{B})}{\partial \ln(x)}$	$\partial_x \mathcal{S} = \frac{\partial \mathcal{S}}{\partial \ln(x)}$
r	1	0
K	$\frac{1}{\kappa - 1}$	$-\frac{\kappa}{\rho - 1}$
a	$\frac{1}{\kappa - 1}$	$-\frac{\kappa}{\rho - 1}$
h	$-\frac{1}{(\rho - 1)(\kappa - 1)}$	$\frac{\kappa(1-\rho) + 2\rho}{(\rho - 1)^2}$
e	$\frac{\rho}{(\rho - 1)(\kappa - 1)} + 1$	$-\frac{2\rho}{(\rho - 1)^2}$
m	$-\frac{\rho}{(\rho - 1)(\kappa - 1)} - 1$	$\frac{2\rho}{(\rho - 1)^2}$

960

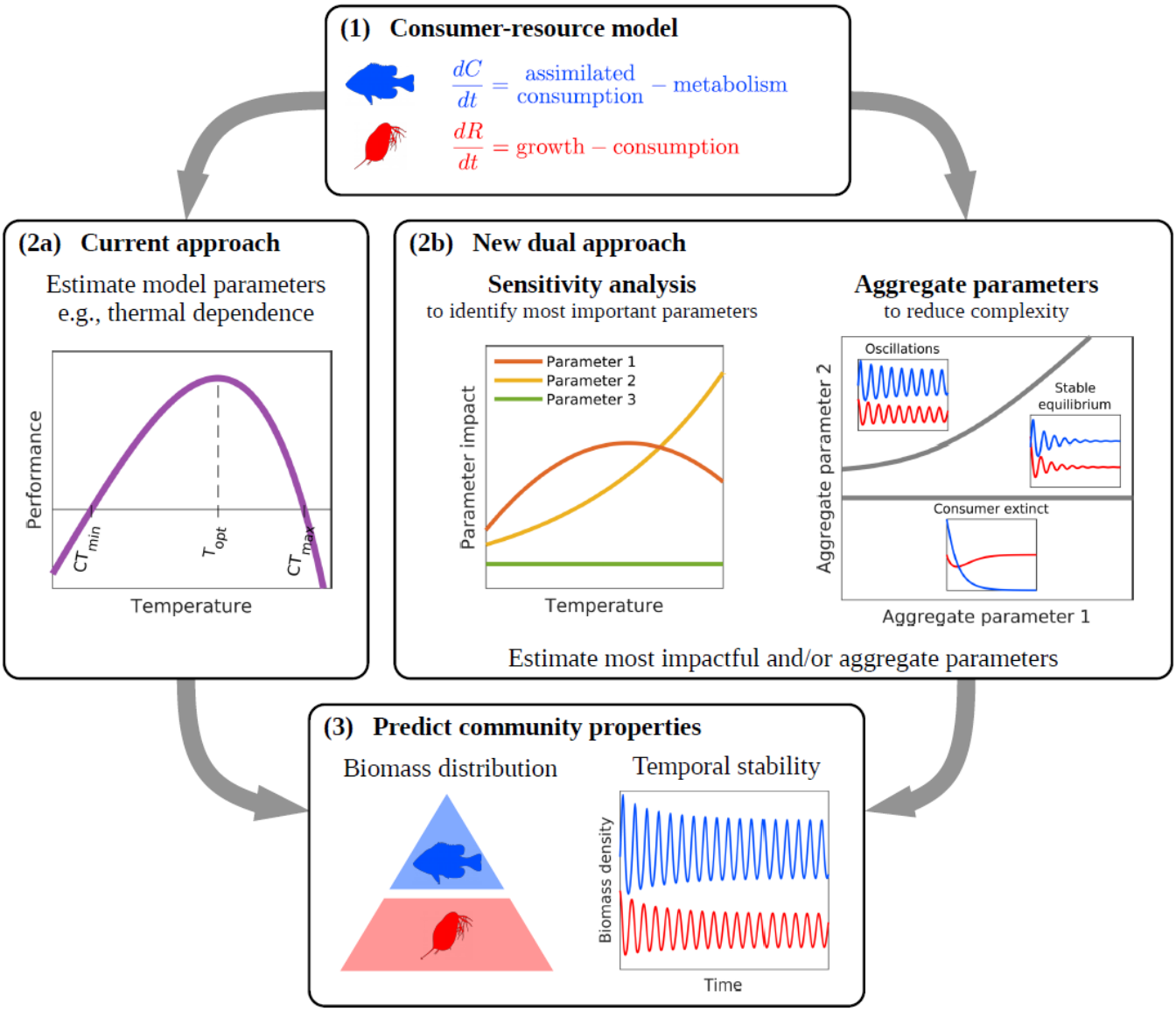

961

962

963 Figure 1. Illustration of the current and new dual approaches to predict the impact of global
964 change drivers on community properties. 1) Predictions require a consumer-resource model;
965 the Rosenzweig-MacArthur model (Rosenzweig & MacArthur 1963) or its bioenergetic
966 equivalent (Yodzis & Innes 1992) have been used most commonly for ectotherm consumer-
967 resource pairs. 2a) The current approach is to experimentally measure the response of
968 parameters along an environmental gradient, e.g. the thermal dependence of the resource
969 population maximal growth rate with critical temperatures, CT_{min}, CT_{max}, and the thermal

optimum, T_{opt}. These measurements are used to parameterise the model. Importantly, not all parameters are measured, but rather those which are considered significant (e.g. consumer feeding and metabolic rates for warming-stability relationships). Assuming the remaining parameter values, the model is then used to generate predictions. 2b) Our new dual approach aims to increase the accuracy of predictions and facilitate their comparison. First a sensitivity analysis determines which parameters have the greatest relative impact on the community property of interest along the environmental gradient. Then, aggregate parameters which represent biologically measurable quantities are used to express all sensitivities and determine the dynamics. Collapsing analyses to the two aggregate parameters reduces complexity and increases mechanistic tractability. This facilitates the choice of which parameters need to be measured. 3) Through the empirical determination of the most appropriate parameters (either from the original model parameters of the aggregate parameters themselves) and the reduction in the number of measurements required, prediction accuracy improves. The advantages of the new dual approach are twofold. First, as the sensitivity analysis will have identified the most impactful parameters, the source of divergence in predictions can be isolated. Second, the aggregates represent standardised measurable population-level indicators across systems, making theoretical or empirical predictions directly comparable.

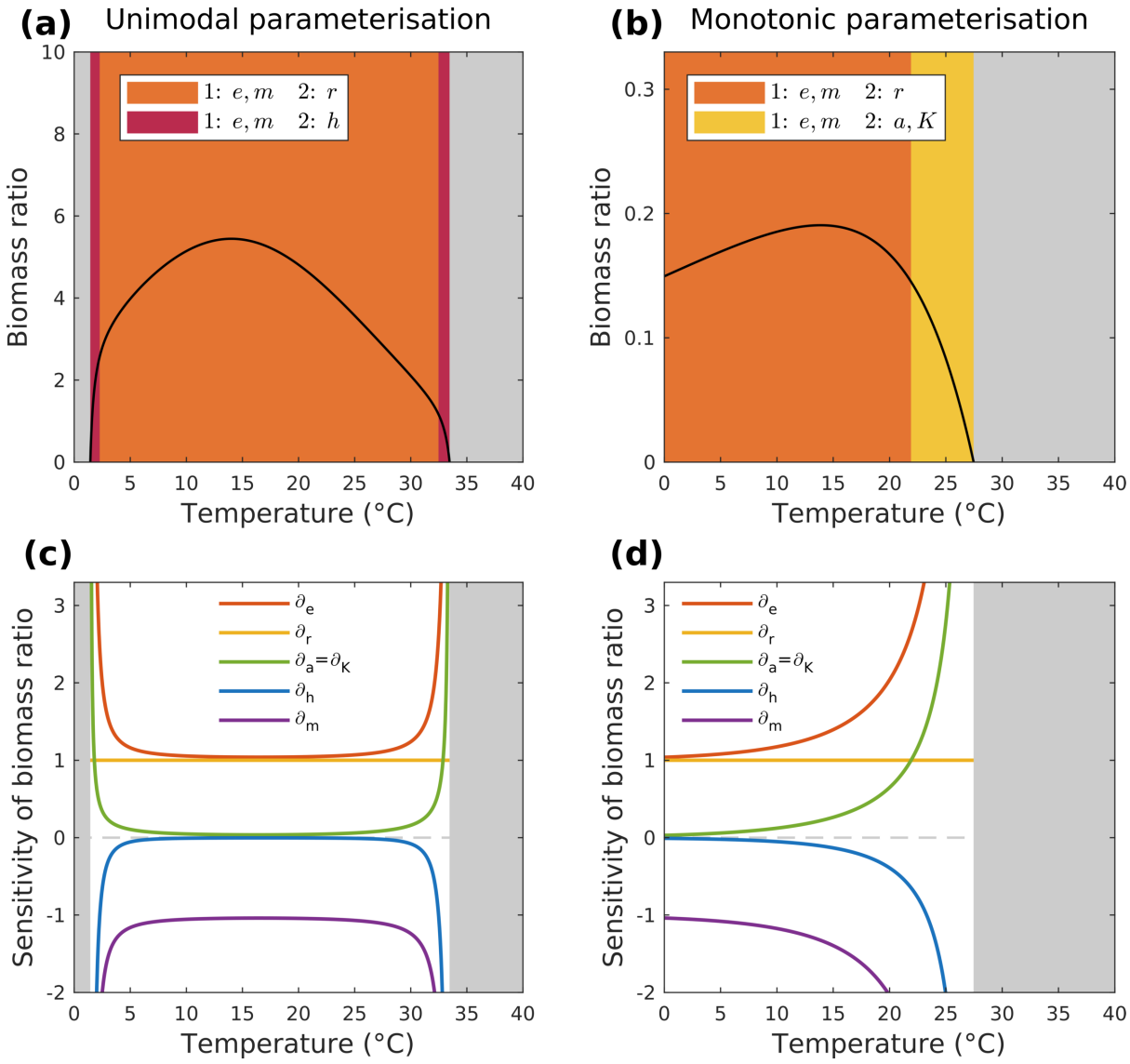

Figure 2. Consumer-resource biomass ratios for the (a) unimodal and (b) monotonic parametrisations along the temperature gradient. Feasible temperature ranges are constrained by the condition of positive biomass densities for both consumer and resource (grey areas correspond to consumer extinction). The different background colours correspond to different elasticity rankings of model parameters (see legend). Panels (c) and (d) provide the values of the six parameter elasticities along the temperature gradient for the unimodal and monotonic parameterisations, respectively.

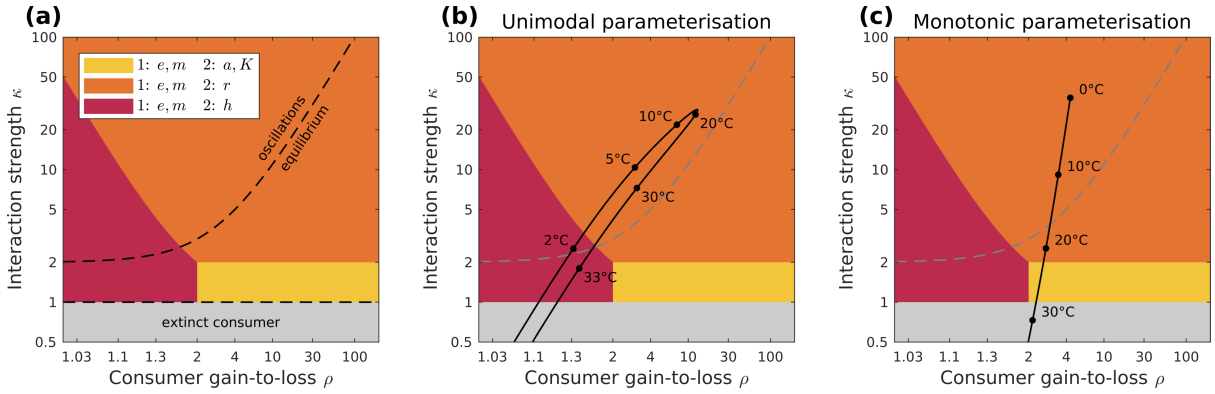

Figure 3. (a) Biomass ratio elasticity rankings in the ρ-κ plane. The plane is split into regions (different colours) which correspond to different parameters having the top-two largest elasticities. These regions have been derived from the analytic expressions of the elasticities (Table 1). e and m elasticities always rank first. Close to consumer extinction h ranks second highest at low ρ ($\rho < 2$, red region) and a and K at higher ρ ($\rho > 2$, yellow region). r ranks second highest far from consumer extinction (orange region). The plane includes the feasibility boundary (κ=1) and the Hopf bifurcation (dotted curve splitting the plane into stable equilibrium and oscillations). For the (b) unimodal and (c) monotonic parameterisations from the literature, the thermal dependencies of $\rho = \frac{e}{mh}$ and $\kappa = \frac{K}{R_S}$ were calculated. This yielded a trajectory for each parameterisation (solid black line). The paths of the trajectories demonstrate the elasticity of the biomass ratio along the temperature gradient for each parameterisation.

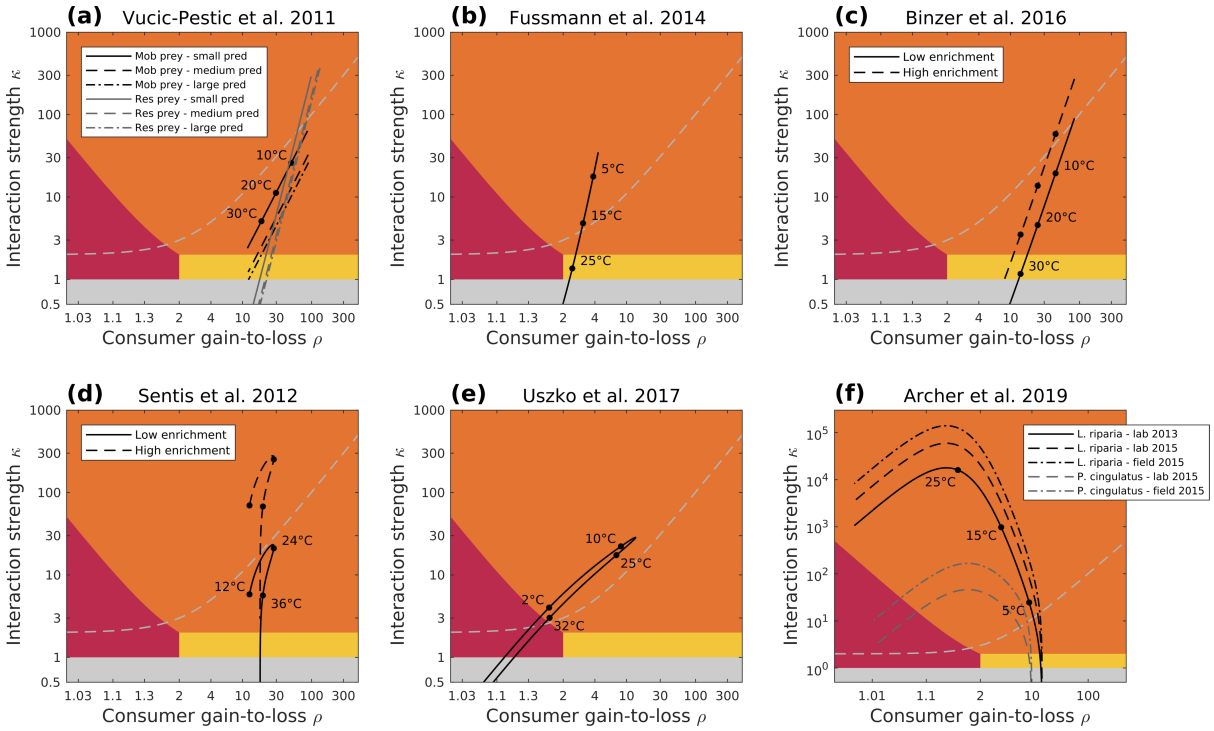

Figure 4. Trajectories of the six empirical temperature parameterisations in the ρ-κ plane: a) Vucic-Pestic *et al.* (2011) with six different experiments – three predator size-classes and two types of prey, b) Fussmann *et al.* (2014), c) Binzer *et al.* (2016) with two levels of enrichment, d) Sentis *et al.* (2012), with two levels of enrichment, e) Uszko *et al.* (2017), f) Archer *et al.* (2019) with two prey types and three measurements. (a), (b) and (c) have monotonic thermal dependences for *a, m* (increasing) and *h, K* (decreasing), and a constant *e*. (d) has a unimodal thermal performance curve for *a* (hump-shaped), constant *e* and *K*, monotonic *h* (decreasing) and *m* (increasing). (e) has a unimodal (U-shaped) *h* and *a* (hump-shaped) thermal dependence, constant *e* and monotonic *K, m* (increasing). (f) has monotonic *a, K, m, e* (increasing) and *h* constant. All parameter values are detailed in SI 4. The coloured regions demonstrate the different biomass ratio sensitivity rankings (see legend in Fig. 3a). The trajectories (solid black lines) for each parameterisation are derived from calculating the thermal dependence of $\rho = \frac{e}{mh}$ and $\kappa = \frac{K}{R_S}$ (see *Temperature dependencies and parameterisations* for details).

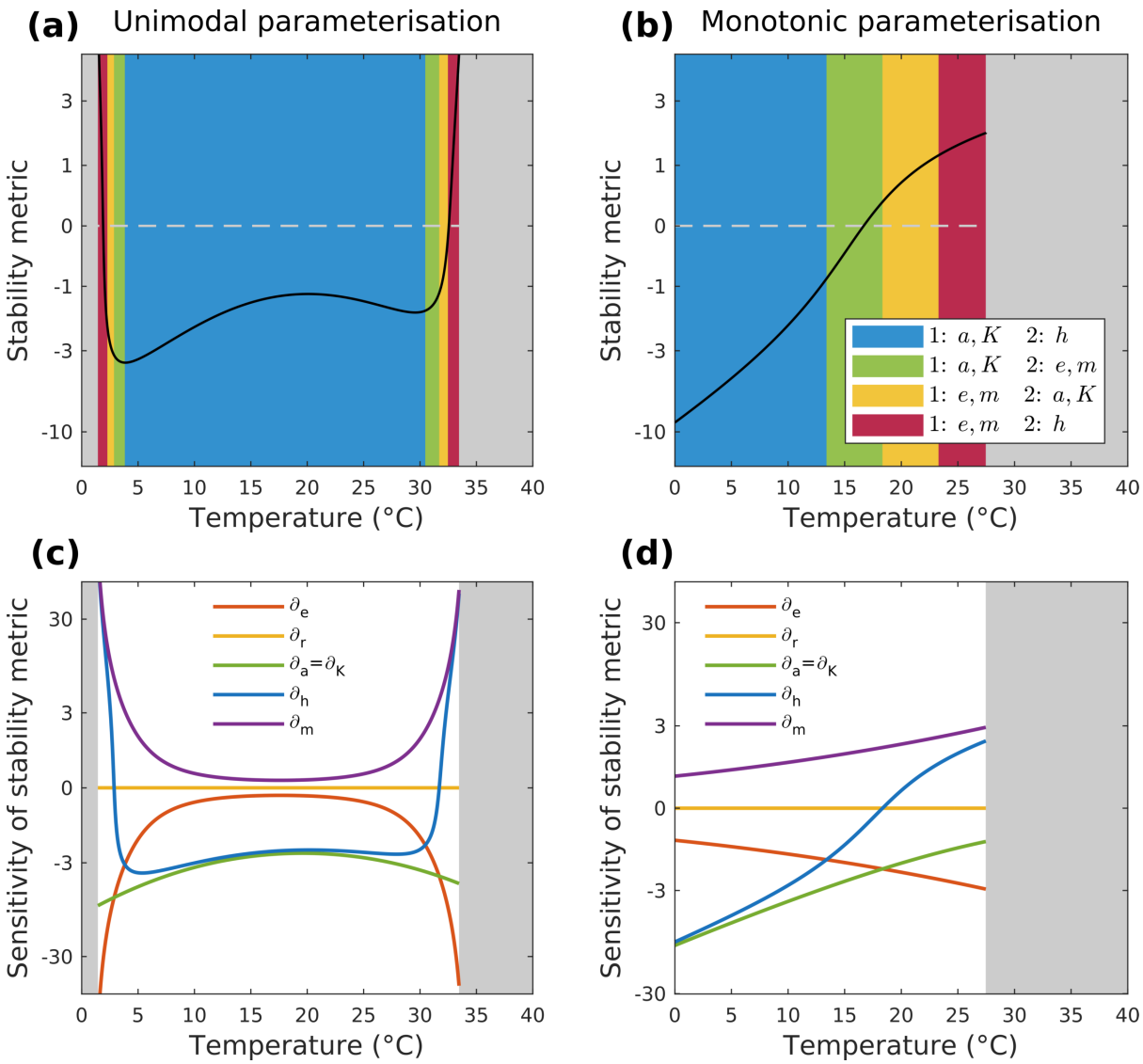

Figure 5. The thermal dependence of the stability metric, $\mathcal{S}$, for the (a) unimodal and (b) monotonic parameterisations. $\mathcal{S} > 0$ corresponds to stable dynamics, $\mathcal{S} < 0$ to oscillations. $\mathcal{S} = 0$ (dotted line) corresponds to the Hopf bifurcation. The coloured temperature ranges highlight regions of different sensitivity rankings. For temperatures beyond the community feasibility boundaries the areas are greyed out. In (c) and (d) the sensitivity to each parameter is plotted along the temperature gradient for the unimodal and monotonic parameterisations, respectively.

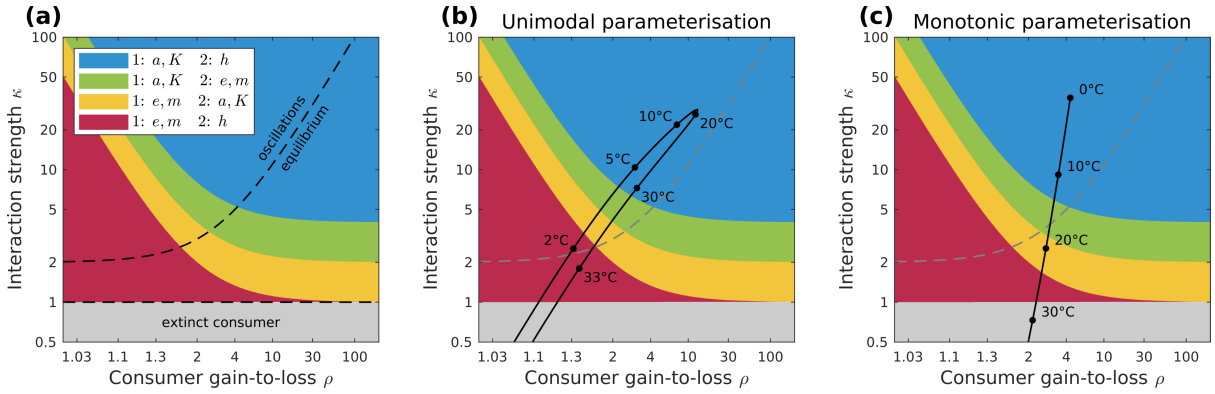

Figure 6. (a) Stability metric sensitivity rankings in the ρ-κ plane. The plane is split into regions (different colours) which correspond to different parameters having the top-two largest sensitivities. These regions have been derived from the analytic expressions of the elasticities (Table 1). *e* and *m* rank first close to consumer extinction; *h* ranks second highest closest to consumer extinction (red region). The sensitivity of stability to *a* and *K* increases moving away from consumer extinction. *a* and *K* sensitivity ranks second (yellow region), and then first moving further away. Initially *e* and *m* rank second (green region) before *h* becomes significant (blue region). The plane includes the feasibility boundary (κ=1) and the Hopf bifurcation (dotted curve splitting the plane into stable equilibrium and oscillations). For the (b) unimodal and (c) monotonic parameterisations from the literature, the thermal dependencies of $\rho = \frac{e}{mh}$ and $\kappa = \frac{K}{R_S}$ were calculated. This yielded a trajectory for each parameterisation (solid black line). The paths of the trajectories demonstrate the dynamical regime and the sensitivity of the stability metric along the temperature gradient for each parameterisation.

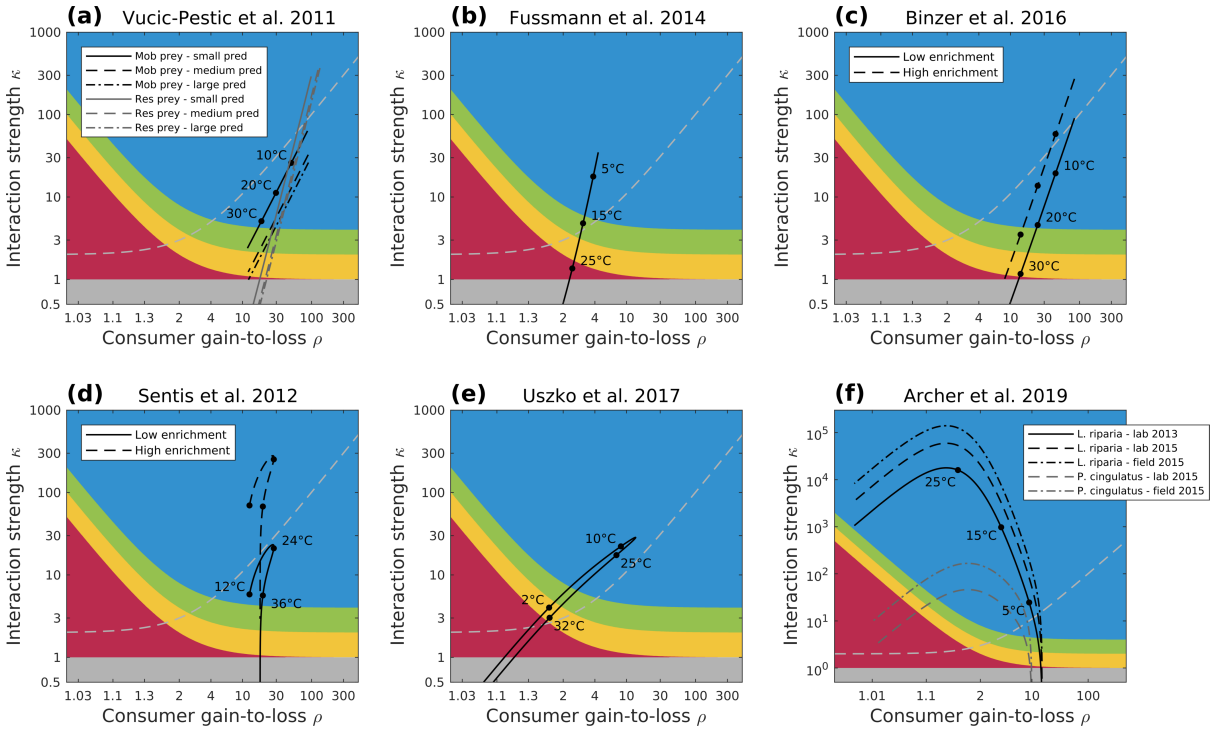

Figure 7. Trajectories of the six empirical temperature parameterisations in the ρ-κ plane: a) Vucic-Pestic *et al.* (2011) with six different interaction experiments – three predator size-classes and two types of prey, b) Fussmann *et al.* (2014), c) Binzer *et al.* (2016) with two levels of enrichment, d) Sentis *et al.* (2012), with two levels of enrichment, e) Uszko *et al.* (2017), f) Archer *et al.* (2019) with two prey types and three measurements. (a), (b) and (c) have monotonic thermal dependences for *a, m* (increasing) and *h, K* (decreasing), and a constant *e*. (d) has a unimodal thermal performance curve for *a* (hump-shaped), constant *e* and *K*, monotonic *h* (decreasing) and *m* (increasing). (e) has a unimodal (U-shaped) *h* and *a* (hump-shaped) thermal dependence, constant *e* and monotonic *K, m* (increasing). (f) has monotonic *a, K, m, e* (increasing) and *h* constant. All parameter values are detailed in SI 4. The coloured regions demonstrate the different biomass ratio sensitivity rankings (see legend in Fig. 6a). The trajectories (solid black line) for each parameterisation are derived from calculating the thermal dependence of $\rho = \frac{e}{mh}$ and $\kappa = \frac{K}{R_S}$. Therefore, trajectories do not change with the variable of interest; the sensitivity regions do.